Logarithmic spiral trajectories generated by solar sails

Marco Bassetto, Lorenzo Niccolai, Alessandro A. Quarta*, Giovanni Mengali

Dipartimento di Ingegneria Civile e Industriale, University of Pisa, I-56122 Pisa, Italy

Abstract

Analytic solutions to low-thrust propelled trajectories are available in a few cases only. An interesting case is offered by the logarithmic spiral, that is, a trajectory characterized by a constant flight path angle and a fixed thrust vector direction in an orbital reference frame. The logarithmic spiral is important from a practical point of view, because it may be passively maintained by a solar sail-based spacecraft. The aim of this paper is to provide a systematic study concerning the possibility of inserting a solar sail-based spacecraft into a heliocentric logarithmic spiral trajectory without using any impulsive maneuver. The required conditions to be met by the sail in terms of attitude angle, propulsive performance, parking orbit characteristics and initial position are thoroughly investigated. The closed-form variations of the osculating orbital parameters are analyzed, and the obtained analytical results are used for investigating the phasing maneuver of a solar sail along an elliptic heliocentric orbit. In this mission scenario, the phasing orbit is composed of two symmetric logarithmic spiral trajectories joined with a coasting arc.

Keywords: solar sail · logarithmic spiral trajectories · orbit phasing

1. Introduction

Solar sailing is one of the most promising innovations among low thrust propulsion systems. Recently, the successes of JAXA's IKAROS mission [24, 16, 8], NASA's NanoSail D-2 [11], and LightSail-1 mission [22, 3], have confirmed the potentialities of solar sail technology and renewed interest for future space applications. In this context, JAXA is currently developing a solar sail aimed at propelling a large-size spacecraft towards Jupiter and the Trojan Asteroids [7]. The estimated propulsion system is a so-called solar power sail, that is, a square $2500\,\mathrm{m}^2$ thin membrane exposed to sunlight, which should guarantee both the required (photonic) propulsive acceleration and supply the electric power necessary to operate an ion engine. Another interesting mission concept involving solar sailing is offered by NASA's Near Earth Asteroid (NEA) Scout [15, 10], whose mission target is the exploration of an asteroid, orbiting in the Earth's vicinity, with a diameter less than 100 m. In this case, the solar sail-based spacecraft is a 6U CubeSat, equipped with a cold gas thruster that should generate the initial impulse necessary for inserting the vehicle on a transfer trajectory. After this maneuver, an $83\,\mathrm{m}^2$ solar sail is intended for supplying the required propulsive acceleration during the cruising phase. Finally, the Planetary Society is planning the launch of LightSail-2 [4], a 3U CubeSat aimed at testing the capability of an orbit raising in a geocentric scenario by means of a $32\,\mathrm{m}^2$ square solar sail.

In a preliminary mission design phase, the trajectory analysis of a spacecraft propelled by a solar sail is a crucial point, which is usually addressed through a numerical integration of the equations of motion. In most cases, a number of possible trajectories must be simulated in order to identify the best option (based on mission requirements), with a non-negligible computational cost. The latter could be significantly reduced by means of closed-form analytical solutions, which represent a very useful tool for mission analysis purposes.

*Corresponding author

Email addresses: marco.bassetto@ing.unipi.it (Marco Bassetto), lorenzo.niccolai@ing.unipi.it (Lorenzo Niccolai), a.quarta@ing.unipi.it (Alessandro A. Quarta), g.mengali@ing.unipi.it (Giovanni Mengali)

Published in Celestial Mechanics and Dynamical Astronomy, Vol. 130, No. 2, 2018. doi: http://doi.org/10.1007/s10569-017-9812-6

In this context, [17] have recently proposed an approximate solution for the two-dimensional trajectory of a solar sail with an asymptotic series expansion, suited for a low-performance propulsion system.

Actually, an exact solution of the equations of motion for a solar sail-based spacecraft exists, and is given by the logarithmic spiral trajectory. More precisely, this solution does not require specific assumptions about the sail performance, and the trajectory is characterized by a constant flight path angle and a fixed thrust orientation [12]. A fixed sail attitude in an orbital reference frame can be passively maintained by a suitable design of both the solar sail shape and the location of its center of mass, thus providing an extremely simple control law for a logarithmic spiral trajectory. The main drawback of the logarithmic spiral is its poor flexibility, since it prevents some important mission scenarios from being feasible, including a circle-to-circle orbit transfer and, more generally, a modification of the initial osculating orbit eccentricity.

The possibility of generating a logarithmic spiral trajectory with a solar sail can be tracked back to the works of [1] and [23]. [26] extended this concept, deriving a three-dimensional form of logarithmic spiral. Later, [25] proposed a circle-to-circle orbit transfer by means of a trajectory composed of a logarithmic spiral arc and two branches connecting it with the parking and the target orbits. [27] introduced a new phase space approach capable of describing the two-dimensional trajectories of a solar sail with a fixed attitude in an orbital reference frame, including the logarithmic spiral. More recently, [19] analyzed the problem of continuous thrust-trajectories, making a useful distinction between different types of spirals, where the logarithmic shape is treated as a special case. The aim of this work is to provide a thorough discussion of heliocentric logarithmic spiral trajectories generated by a solar sail. Unlike existing literature, the focus here is on the constraints to be met by a spacecraft in order to be placed in a logarithmic spiral trajectory without any impulsive maneuver. In addition, assuming a flat sail, the mathematical model discussed in this paper shows, for the first time, an interesting correlation between the logarithmic spiral characteristics (or the osculating orbital parameters), and the thermo-optical parameters that describe the sail force model [28, 13]. The use of a thrust model related to the actual optical characteristics of the sail reflective film represents an innovation in the logarithmic spiral trajectory analysis, since, so far, the problem has been addressed under the simplifying assumption of specularly reflective sail only, that is, with an ideal force model.

The paper is organized as follows. Starting from a brief discussion on two-dimensional polar equations of motion and solar sail thrust models, the next section derives the analytical relations describing the sail dynamics, the variations of the orbital parameters, and the constraints related to the initial conditions. Section 3 presents a potential application of the logarithmic spiral to the problem of orbit phasing in a heliocentric mission scenario. The last section gives some concluding remarks and summarizes the main outcomes of the work.

2. Solar sail insertion into a logarithmic spiral trajectory

Consider a spacecraft, initially placed on a heliocentric Keplerian orbit with eccentricity e_0 and semimajor axis a_0, which deploys a solar sail at time $t = t_0 \triangleq 0$, when the spacecraft true anomaly is $\nu_0 \in [0,\, 360]$ deg. The solar sail provides a continuous thrust that is used to modify the vehicle trajectory. The problem is to investigate the conditions required to insert the spacecraft into a logarithmic spiral trajectory without the need for any impulsive maneuver.

To proceed, consider the spacecraft equations of motion in a heliocentric polar reference frame $\mathcal{T}(O; r, \theta)$, which are given by

$$\dot{r} = v_r, \tag{1}$$

$$\dot{\theta} = \frac{v_\theta}{r}, \tag{2}$$

$$\dot{v}_r = -\frac{\mu_\odot}{r^2} + \frac{v_\theta^2}{r} + \beta\,\frac{\mu_\odot}{r^2}\,R, \tag{3}$$

$$\dot{v}_\theta = -\frac{v_r\, v_\theta}{r} + \beta\,\frac{\mu_\odot}{r^2}\,T, \tag{4}$$

where $\mu_\odot$ is the Sun's gravitational parameter, r is the Sun-spacecraft distance, θ is the angular coordinate measured counterclockwise from the direction of the parking orbit eccentricity vector (that is, $\theta_0 = \nu_0$,

see Fig. 1), and v_r (v_θ) is the radial (transverse) component of the spacecraft velocity. In Eqs. (1)–(4), the dot indicates the derivative with respect to time. The last terms in Eqs. (3)-(4) model the solar sail

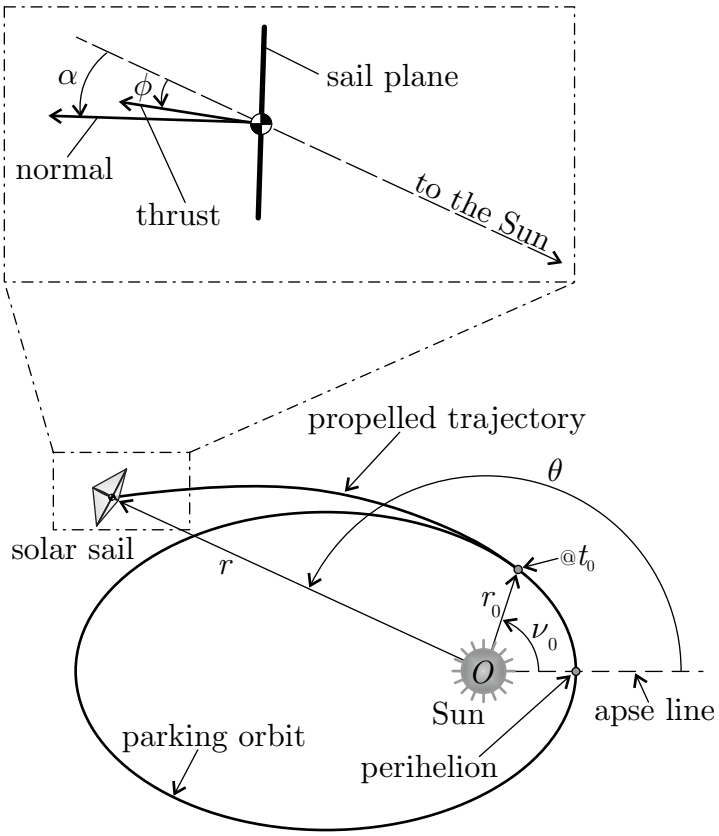

Figure 1: **Reference frame and characteristics angles α and ϕ.**

propulsive acceleration, where β, referred to as lightness number, is the (constant) ratio of the maximum magnitude of propulsive acceleration to the local solar gravitational acceleration at a given heliocentric distance r [13], while R and T are the dimensionless radial and transverse components of the solar-sail propulsive acceleration.

2.1. Solar sail force model

The conditions required to insert a solar sail-based spacecraft into a logarithmic spiral trajectory depend on the model used to describe the solar sail thrust. A common choice in a preliminary mission design is to assume a flat sail with an optical force model [28, 13], in which the dimensionless radial (R) and transverse (T) components of the solar sail propulsive acceleration are

$$R = \cos\alpha \left(b_1 + b_2 \cos^2 \alpha + b_3 \cos\alpha\right), \tag{5}$$

$$T = \cos\alpha \sin\alpha \left(b_2 \cos\alpha + b_3\right), \tag{6}$$

where $\alpha \in [-90, 90]$ deg is the sail pitch angle, that is, the angle between the Sun-spacecraft line and the direction of the unit vector perpendicular to the sail surface and directed away from the Sun, see Fig. 1. Note that the thrust vector direction is constant in an orbital reference frame only if α is constant. The coefficients b_1, b_2, and b_3 in Eqs. (5) and (6), referred to as force coefficients, depend on the optical characteristics of

the sail reflective film, and are defined as [17]

$$b_1 = \frac{1-\rho\, s}{2}, \tag{7}$$

$$b_2 = \rho\, s, \tag{8}$$

$$b_3 = \frac{B_f\, \rho\, (1-s)}{2} + \frac{(1-\rho)\ (\epsilon_f\, B_f - \epsilon_b\, B_b)}{2\ (\epsilon_f + \epsilon_b)}, \tag{9}$$

where ρ is the reflection coefficient, s is the fraction of photons that are specularly reflected, B_f (or B_b) is the non-Lambertian coefficient of the front (or back) sail surface, ϵ_f (or ϵ_b) the emissivity coefficient of the front (or back) sail surface. In particular, when the degradation of the sail reflective film is neglected [6, 5], b_1, b_2, and b_3 are all constant. For example, for an ideal sail, characterized by a perfectly specular reflection of light and a zero absorption coefficient, the force coefficients are $b_1 = b_3 = 0$ and $b_2 = 1$. Assuming, instead, a typical sail film with a highly reflective aluminum-coated front side and a highly emissive chromium-coated back side [13], the values of the force coefficients are $b_1 = 0.0723$, $b_2 = 0.8554$, and $b_3 = -0.003$, in accordance with the recent results by [9]. Note that the maximum (minimum) value of the dimensionless transverse propulsive acceleration T is about 0.3278 (-0.3278), and occurs when $\alpha \simeq 35.2\,\text{deg}$ ($\alpha \simeq -35.2\,\text{deg}$), see Fig. 2.

For the analysis to follow, it is useful to introduce an auxiliary function $P = P(\alpha)$, defined as the ratio of the transverse to the radial component of the dimensionless propulsive acceleration, viz.

$$P \triangleq \frac{T}{R} = \frac{\sin\alpha\,(b_2\,\cos\alpha + b_3)}{b_1 + b_2\,\cos^2\,\alpha + b_3\,\cos\alpha}. \tag{10}$$

Note that $P = \tan\phi$, where ϕ is the thrust angle, that is, the angle between the Sun-spacecraft line and the sail thrust direction, see Fig. 1. For an ideal sail $P(\alpha) \equiv \tan(\alpha)$, therefore P increases monotonically with α and, in this case, the pitch angle α coincides with the thrust angle ϕ. On the other hand, for an optical force model $\phi < \alpha$ (with the only exception of a Sun-facing sail in which $\alpha = \phi = 0$), and P has a single positive stationary point at $\alpha = \alpha^\star > 0$, where P takes its maximum value $P_{\max} = P(\alpha^\star)$, with

$$P_{\max} = P(\alpha^\star) = \frac{(3\,b_1\,b_3 + d)\ \sqrt{1 - \dfrac{g^2}{4\,b_2^2\ (2\,b_1 + b_2)^2}}}{2\ (2\,b_1 + b_2)\ \left[b_1 + \dfrac{g^2}{4\,b_2\ (2\,b_1 + b_2)^2} - \dfrac{b_3\,g}{2\,b_2\ (2\,b_1 + b_2)}\right]} \tag{11}$$

and

$$\alpha^\star = \arccos\left(-\frac{g}{2\,b_2\ (2\,b_1 + b_2)}\right), \tag{12}$$

where

$$d \triangleq \sqrt{b_1\,(4\,b_2^3 + 8\,b_1\,b_2^2 - 4\,b_2\,b_3^2 + b_1\,b_3^2)}, \tag{13}$$

$$g \triangleq b_1\,b_3 + 2\,b_2\,b_3 - d. \tag{14}$$

In particular, using the force coefficients $\{b_1, b_2, b_3\}$ calculated with the results by [9], it may be verified that $\alpha^\star \simeq 74.2\,\text{deg}$ and $P_{\max} \simeq 1.64$, see Fig. 3. Note that $P(\alpha)$ is an odd function of α, and its minimum value is $P_{\min} = -P_{\max} = P(-\alpha^\star)$.

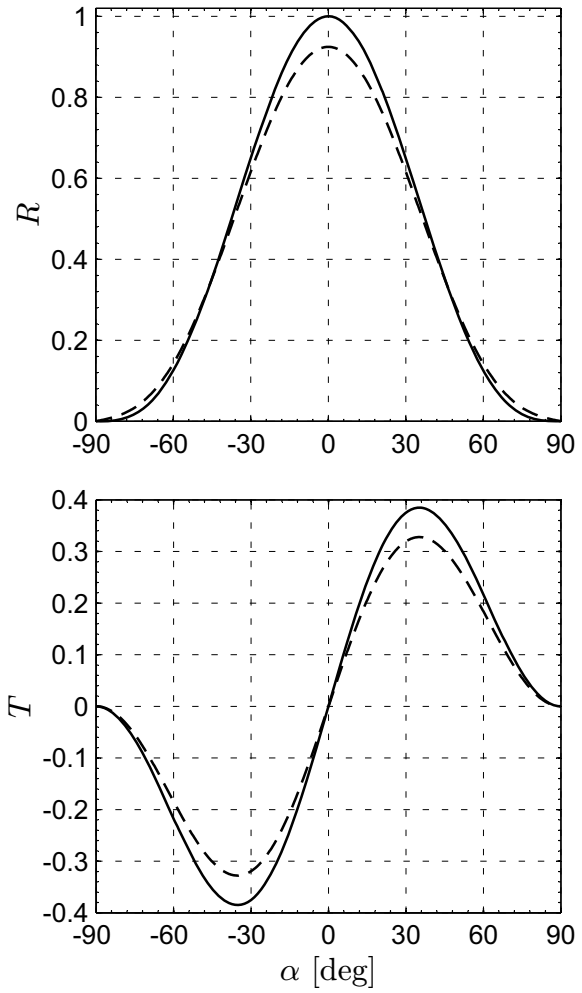

Figure 2: **Dimensionless components of propulsive acceleration as a function of the pitch angle for a flat solar sail with an ideal (solid line) and optical (dash line, data taken from [9]) force model.**

2.2. Logarithmic spiral trajectory

According to [18], when a spacecraft covers a heliocentric logarithmic spiral, its distance from the Sun can be written as a function of the angular coordinate θ as

$$r(\theta) = r_0 \, \exp\left[\tan\gamma \, (\theta - \nu_0)\right], \tag{15}$$

where

$$r_0 \triangleq r(\theta_0) \equiv r(\nu_0) = \frac{a_0 \, \left(1 - e_0^2\right)}{1 + e_0 \, \cos\nu_0} \tag{16}$$

is the Sun-spacecraft distance at time t_0, and γ is a constant parameter that coincides with the flight path angle. To avoid the need of an additional (chemical) propulsion system, the spacecraft is assumed to leave the parking orbit without any impulsive maneuver, that is, its velocity at $t = t_0$ (when the sail is deployed) coincides with the Keplerian velocity on the parking orbit. Accordingly, the flight path angle is related to the parking orbit characteristics by

$$\tan\gamma = \frac{e_0 \sin\nu_0}{1 + e_0 \cos\nu_0} \tag{17}$$

and is therefore a function of the pair $\{e_0, \, \nu_0\}$.

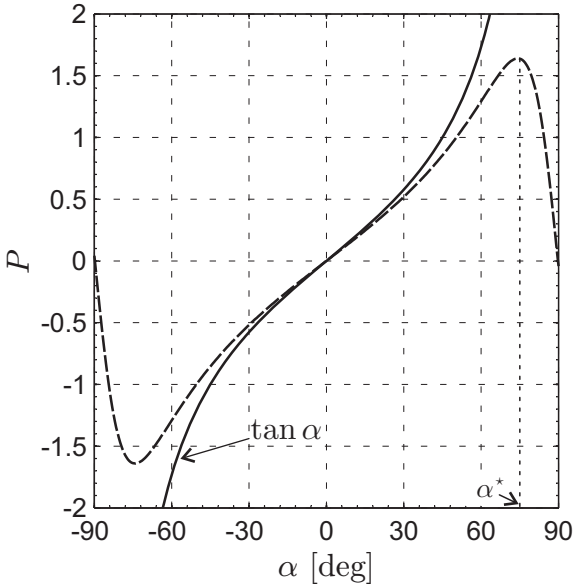

Figure 3: **Ratio P between the dimensionless components of propulsive acceleration as a function of the pitch angle, see Eq.** (10)**. Ideal (solid line) and optical (dash line, data taken from [9]) force model.**

In order to calculate the spacecraft velocity components along a logarithmic spiral trajectory, recall that the radial velocity component v_r and its time-derivative $\dot{v}_r$ can be written as

$$v_r = \frac{\mathrm{d}r}{\mathrm{d}\theta}\,\dot{\theta} = r\,\dot{\theta}\,\tan\gamma = v_\theta\,\tan\gamma, \qquad\qquad \dot{v}_r = \dot{v}_\theta\,\tan\gamma. \tag{18}$$

Paralleling the procedure described by [13], Eqs. (18) can be specialized to the case of logarithmic spiral covered by a solar sail spacecraft. In fact, when Eqs. (18) are substituted into Eqs. (3)-(4), the radial and transverse components of the spacecraft velocity become

$$v_\theta = r\,\frac{\mathrm{d}\theta}{\mathrm{d}t} = k\,\sqrt{\frac{\mu_\odot}{r}}\,\cos\gamma, \tag{19}$$

$$v_r = \frac{\mathrm{d}r}{\mathrm{d}t} = k\,\sqrt{\frac{\mu_\odot}{r}}\,\sin\gamma, \tag{20}$$

where

$$k \triangleq \sqrt{1+\beta\,T\,\tan\gamma - \beta\,R}. \tag{21}$$

The magnitude $v = \sqrt{v_r^2 + v_\theta^2}$ of the heliocentric velocity is therefore

$$v = k\,\sqrt{\frac{\mu_\odot}{r}}. \tag{22}$$

Note that the dimensionless constant parameter k coincides with the ratio of the solar sail velocity along the logarithmic spiral trajectory to its local circular velocity. Therefore, it takes positive values only. It will be shown later that k may be written as a function of the pair $\{e_0,\,\nu_0\}$, and that $k < 1$ on a closed parking orbit.

2.3. Osculating orbit characteristics

The characteristics of the spacecraft osculating orbit, in terms of semimajor axis a, eccentricity e, and direction of eccentricity vector, can be obtained as a function of the heliocentric distance r using Eqs. (19)-

(20). In fact, since the magnitude of the specific angular momentum vector is $h = r\,v_\theta = k\,\cos\gamma\,\sqrt{\mu_\odot\,r}$, the semilatus rectum p of the osculating orbit is found to be proportional to r (that is, p varies exponentially with the angular coordinate θ) through the following relationship

$$p = r\,k^2\,\cos^2\gamma, \tag{23}$$

where k is given by Eq. (21). From the specific mechanical energy equation, and recalling Eqs. (19)-(20), the semimajor axis of the osculating orbit is

$$a = \frac{r}{2 - k^2}. \tag{24}$$

Note that, from Eqs. (23)-(24), the ratio p/a and r/p are constant and, therefore, both the eccentricity e and the true anomaly ν of the osculating orbit are constants of motion, viz.

$$e = e_0, \qquad\qquad \nu = \nu_0. \tag{25}$$

Also, from this last equation, the angle ω between the osculating orbit eccentricity vector and the parking orbit eccentricity vector is given by

$$\omega = \theta - \nu_0, \tag{26}$$

which corresponds to the rotation angle of the osculating orbit apse line, measured counterclockwise from the eccentricity vector of the parking orbit. It is worth noting that the results obtained in this section, expressed by Eqs. (23)–(26), are valid for solar sail-based spacecraft only, and cannot be used for a generic vehicle that covers a logarithmic spiral trajectory.

Finally, from Eqs. (15) and (25), the semimajor axis of the osculating orbit may be explicitly written as a function of the angular coordinate θ as

$$a = a_0\,\exp\left[\tan\gamma\,(\theta - \theta_0)\right]. \tag{27}$$

Likewise, combining Eqs. (25) and (27), the variation of p with θ is

$$p = p_0\,\exp\left[\tan\gamma\,(\theta - \nu_0)\right], \tag{28}$$

where $p_0 = a_0\,(1 - e_0^2)$ is the semilatus rectum of the parking orbit.

2.4. Propulsive requirements

The problem now is to find the propulsive requirements necessary for a solar sail-based spacecraft to move along a given logarithmic spiral trajectory with a constant pitch angle α, that is, with a fixed thrust vector direction in an orbital reference frame. To that end, consider the time derivative of v_θ, which, bearing in mind Eq. (19), becomes

$$\dot{v}_\theta = \frac{\mathrm{d}v_\theta}{\mathrm{d}r}\,v_r = -\frac{v_\theta\,v_r}{2\,r}. \tag{29}$$

Accordingly, Eq. (4) gives

$$\frac{v_\theta\,v_r}{2} = \beta\,T\,\frac{\mu_\odot}{r}. \tag{30}$$

Substituting Eqs. (19)-(20) into Eq. (30), and taking into account Eq. (21), the result is

$$\frac{\sin 2\gamma}{4} = \frac{\beta\,T}{k^2}. \tag{31}$$

From the trigonometric identity

$$\frac{\sin\left(2\arctan x\right)}{4} = \frac{x}{2\,\left(x^2 + 1\right)} \tag{32}$$

and setting $x = \tan\gamma$ (where $\tan\gamma$ is given by Eq. (17)), an equivalent version of Eq. (31) is

$$\frac{e_0\ \sin\nu_0\ (1+e_0\ \cos\nu_0)}{2\ (1+e_0^2+2\,e_0\ \cos\nu_0)} = \frac{\beta\,T}{k^2}. \tag{33}$$

In addition, when the polar equation of the osculating orbit $r = a\,(1-e_0^2)/(1+e_0\ \cos\nu_0)$ is combined with Eq. (24), the result is

$$k^2 = \frac{1+e_0^2+2\,e_0\ \cos\nu_0}{1+e_0\ \cos\nu_0}, \tag{34}$$

which shows that k is a function of $\{e_0,\ \nu_0\}$ only.

Finally, from Eqs. (33)-(34), and taking into account Eq. (21), the expressions of the augmented components of the radial ($\beta\,R$) and transverse ($\beta\,T$) dimensionless propulsive acceleration are obtained as a function of the pair $\{e_0,\ \nu_0\}$ as

$$\beta\,T = \frac{e_0\ \sin\nu_0}{2}, \tag{35}$$

$$\beta\,R = -\frac{e_0\ \left(e_0\ \cos^2\nu_0+2\ \cos\nu_0+e_0\right)}{2\ (1+e_0\ \cos\nu_0)}, \tag{36}$$

where R and T depend on the sail pitch angle α and the force coefficients $\{b_1,\ b_2,\ b_3\}$ according to Eqs. (5) and (6), respectively. In particular, the sign of pitch angle α (and so the sign of T) coincides with the sign of $\sin\nu_0$, see Eq. (35).

To summarize, for an assigned parking orbit eccentricity e_0 and for a given initial (angular) position ν_0, the solar sail spacecraft covers a logarithmic spiral trajectory only if the lightness parameter β and the pitch angle α are in accordance with Eqs. (35) and (36). Note that, independent of the selected force model, when the parking orbit is circular ($e_0 = 0$), Eqs. (35)–(36) state that $\beta = 0$, that is, the sail thrust is equal to zero. Indeed, it is well known [13] that a solar sail-based spacecraft cannot be inserted into a logarithmic spiral trajectory from a circular parking orbit unless a discontinuity in the vehicle velocity is introduced, which implies the use of an impulsive maneuver just before the sail deployment. This point, of course, imposes a serious limitation on the use of logarithmic spirals as transfer trajectories between coplanar orbit, since it leaves out the noteworthy case of circular orbits of different radius. However, even neglecting the case of circular parking orbit, there exist some limitations on the choice of initial orbital eccentricity and spacecraft position, since not all the pairs $\{e_0,\ \nu_0\}$ turn out to be feasible, as will now be shown.

2.5. Force model constraints

Since the solar sail propulsive acceleration has always an outward radial component with respect to the Sun (regardless of the selected force model), the initial conditions in terms of e_0 and ν_0 must be chosen such that $R \geq 0$. Observing that $\beta > 0$ and $e_0 > 0$, the constraint $R \geq 0$ in Eq. (36) corresponds to enforcing $\left(e_0\ \cos^2\nu_0+2\ \cos\nu_0+e_0\right) < 0$. In particular, when the parking orbit is open, that is, $e_0 \geq 1$ and $\nu_0 \in (-\arccos(1/e_0),\ \arccos(1/e_0))$, the maximum value of R is $-(\sqrt{e_0^2-1})/\beta \leq 0$. This result implies that a solar sail spacecraft cannot be inserted into a logarithmic spiral trajectory starting from an open parking orbit. In addition, the escape conditions cannot be reached along a logarithmic spiral trajectory. Indeed, the orbital velocity goes to zero as the heliocentric distance tends to infinity, see Eq. (22). The latter result is by no means surprising, since the osculating orbital eccentricity does not vary along a logarithmic spiral, see the first of Eqs. (25). On the other hand, when the osculating orbit is elliptical, that is, $e_0 \in (0,\ 1)$ and $\nu_0 \in [0, 2\pi]$, the condition $\beta\,R > 0$ yields

$$\cos\nu_0 \leq \frac{\sqrt{1-e_0^2}-1}{e_0}, \tag{37}$$

which can be equivalently written as

$$\nu_0 \in [\nu_0^\star,\ 2\,\pi-\nu_0^\star] \qquad \text{with} \qquad \nu_0^\star \triangleq \arccos\left(\frac{\sqrt{1-e_0^2}-1}{e_0}\right). \tag{38}$$

From the polar equation of the parking orbit, Eq. (37) can be rearranged as

$$r_0 \geq a_0 \sqrt{1 - e_0^2}, \tag{39}$$

stating that a logarithmic spiral can be covered by a solar sail spacecraft only if the sail is deployed when the heliocentric distance is greater than the semiminor axis of the parking orbit $a_0 \sqrt{1 - e_0^2}$.

Another constraint on the choice of the initial conditions e_0 and ν_0 is obtained recalling that $T/R = P(\alpha)$, see Eq. (10). Taking the ratio of Eq. (35) to Eq. (36), it is found that

$$P(\alpha) = F(e_0, \nu_0) \qquad \text{with} \qquad F(e_0, \nu_0) \triangleq -\frac{\sin\nu_0 \ (1 + e_0 \ \cos\nu_0)}{e_0 \ \cos^2\nu_0 + 2 \ \cos\nu_0 + e_0}. \tag{40}$$

Assuming an ideal force model (i.e. when $b_1 = b_3 = 0$ and $b_2 = 1$), the function $P = P(\alpha)$ has no stationary points, since $P = \tan\alpha$, see Eq. (10). In this case any pair $\{e_0, \nu_0\}$ that meets Eq. (38) is feasible. When an optical force model is used, instead, the function $P = P(\alpha)$ has an absolute minimum $(-P(\alpha^\star))$ and an absolute maximum $(P(\alpha^\star))$, see Fig. 3, which may be obtained from Eq. (11) as a function of the force coefficients $\{b_1, b_2, b_3\}$. In this case, a generic pair $\{e_0, \nu_0\}$ is feasible only if the corresponding value $F(e_0, \nu_0)$, calculated with Eq. (40), satisfies

$$F(e_0, \nu_0) \in [-P(\alpha^\star), P(\alpha^\star)], \tag{41}$$

where $P(\alpha^\star)$ is given by Eq. (11). Equation (41) gives two constraints on the pair $\{e_0, \nu_0\}$, viz.

$$e_0 \leq -\frac{\sin\nu_0 + 2\,P(\alpha^\star) \ \cos\nu_0}{P(\alpha^\star) \ \cos^2\nu_0 + \sin\nu_0 \ \cos\nu_0 + P(\alpha^\star)}, \tag{42}$$

$$e_0 \leq \frac{\sin\nu_0 - 2\,P(\alpha^\star) \ \cos\nu_0}{P(\alpha^\star) \ \cos^2\nu_0 - \sin\nu_0 \ \cos\nu_0 + P(\alpha^\star)}, \tag{43}$$

which must be met along with the inequality of Eq. (37).

From a graphical viewpoint, the constraints of Eq. (37) and Eqs. (42)-(43) mark the boundary of an admissible region in the plane (e_0, ν_0), see Fig. 4, within which the eccentricity of the parking orbit (e_0) and the initial spacecraft position (ν_0) must be selected in order to obtain a logarithmic spiral trajectory. In other terms, for a given parking orbit eccentricity e_0, Fig. 4 defines the range of initial true anomalies consistent with the solar sail characteristics.

Figure 4 also quantifies the considerable reduction (especially in case of small eccentricities) of the admissible region related to a non-ideal sail behavior. For example, assuming a parking orbit with an eccentricity equal to that of Earth's heliocentric orbit, i.e. $e_0 = e_\oplus \triangleq 0.0167$, the admissible range of true anomalies $\nu_0 \in [91, 269]\,\text{deg}$ (ideal sail) reduces to $\nu_0 \in [107, 253]\,\text{deg}$ (optical force model).

Having found an admissible pair $\{e_0, \nu_0\}$ with the aid of Fig. 4, the problem of calculating the required values of sail lightness number β and pitch angle α can be summarized as follows: 1) obtain α by imposing $P(\alpha) = F(e_0, \nu_0)$, where $P(\alpha)$ is given by Eq. (10), 2) find R with Eq. (5), and 3) calculate the required value of β using Eq. (36). In case of ideal force model, this procedure gives an explicit closed-form solution, consistent with the approach by [13], viz.

$$\alpha = \arctan\left[\frac{-\sin\nu_0 \ (1 + e_0 \ \cos\nu_0)}{e_0 + 2 \ \cos\nu_0 + e_0 \ \cos^2\nu_0}\right], \tag{44}$$

$$\beta = \frac{-e_0 \left[\dfrac{\sin^2\nu_0 \, (1 + e_0 \ \cos\nu_0)^2}{(e_0 + 2 \ \cos\nu_0 + e_0 \ \cos^2\nu_0)^2} + 1\right]^{3/2} \left(e_0 + 2 \ \cos\nu_0 + e_0 \ \cos^2\nu_0\right)}{2 \ (1 + e_0 \ \cos\nu_0)}. \tag{45}$$

The lightness number β can be rewritten in a more compact form, using Eq. (44) and recalling that $\cos\alpha \geq 0$,

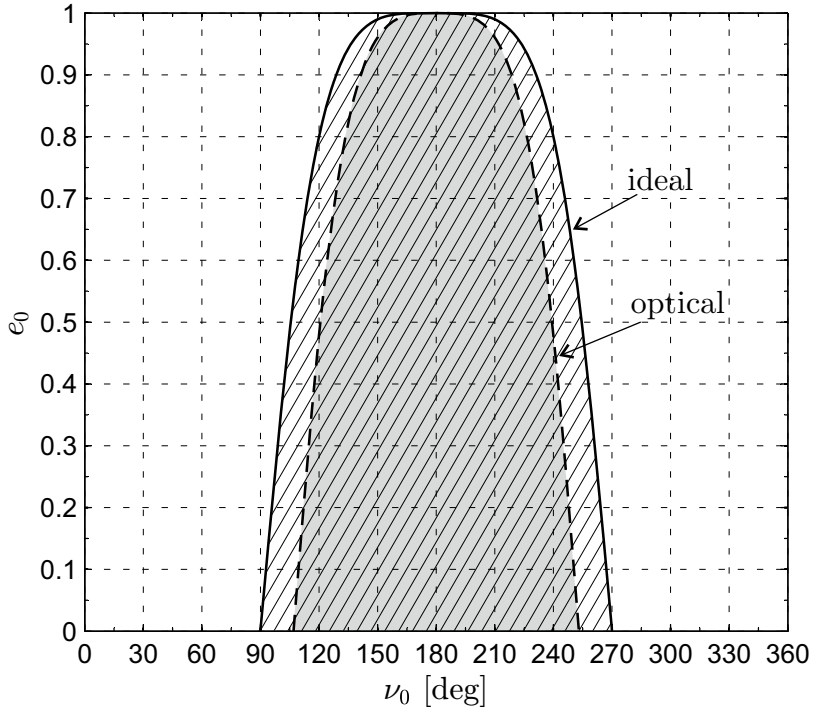

Figure 4: **Admissible pairs $\{e_0, \nu_0\}$ for a flat solar sail with an ideal (hatch area) and optical (grey area) force model.**

viz.

$$\beta = \frac{1}{2} \frac{e_0 \, \sin \nu_0}{\sin \alpha \, \cos^2 \alpha}. \tag{46}$$

From Eq. (46), when $\alpha = \pm 90\,\text{deg}$ (i.e. when the sail thrust goes to zero) the required value of β tends to infinity. In this limiting case the logarithmic spiral cannot be tracked by a solar sail-based spacecraft.

Figure 5 illustrates how the required values of α and β vary with the initial true anomaly ν_0 and the parking orbit eccentricity e_0. Note that, if $\nu_0 = 180\,\text{deg}$, the value of the lightness number is $\beta = e_0$, see also Eq. (45). Moreover, β quickly increases as $|\alpha| \to 90\,\text{deg}$, whereas it has a weak dependence on ν_0 (especially for small values of the eccentricity) when the value of α is sufficiently small.

When an optical force model is used, the previous procedure must account for an additional problem in the evaluation of the pitch angle with Eq. (40). In fact, if $b_1 \neq 0$ and $b_3 \neq 0$, there is not, in general, a single solution to the equation $\alpha = \alpha(P)$. However, with the aid of Fig. 2, it may be easily checked that R is maximized by selecting the minimum admissible value of $|\alpha|$, which, in turn, corresponds to the minimum value of lightness number β, see Eq. (36). The minimum admissible β is clearly the best choice, because, for a given spacecraft mass, a smaller β corresponds to a smaller sail surface. In conclusion, α is to be selected in the range $[-\alpha^\star, \alpha^\star]$, within which P is a monotonically increasing function of the sail pitch angle. A first order approximation, which can be easily refined with standard root finding techniques, is given by

$$\alpha \simeq 1.379 \, \arctan \left[\frac{-0.7548 \, \sin \nu_0 \, (1 + e_0 \, \cos \nu_0)}{e_0 \, \cos^2 \nu_0 + 2 \, \cos \nu_0 + e_0} \right], \tag{47}$$

where α is in radians. Having calculated the pitch angle, the lightness number is obtained from Eq. (36) as

$$\beta = -\frac{e_0 \, \left(e_0 \, \cos^2 \nu_0 + 2 \, \cos \nu_0 + e_0 \right)}{2 \, \cos \alpha \, (1 + e_0 \, \cos \nu_0) \, (b_1 + b_2 \, \cos^2 \, \alpha + b_3 \, \cos \alpha)}. \tag{48}$$

Figure 6 shows the variation of α and β as functions of ν_0 and e_0. The forbidden regions in gray colour are

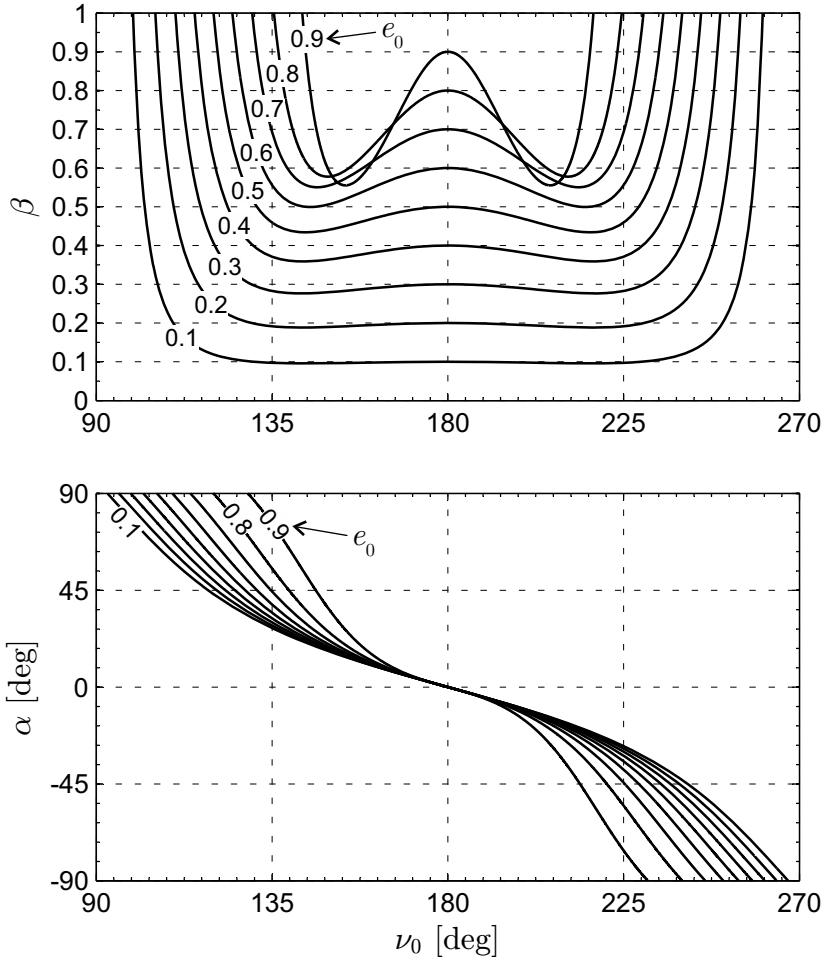

Figure 5: **Required pitch angle α and sail lightness number β as a function of ν_0 and e_0 for an ideal force model.**

associated to the constraints of Eqs. (42)-(43). These forbidden regions are lacking in Fig. 5 since an ideal sail force model allows any value of $\alpha \in [-90,\, 90]\,\text{deg}$ to be feasible. In the noteworthy case of $e_0 = e_\oplus$, the variation of β and α with the pair $\{e_0,\, \nu_0\}$ is drawn in Fig. 7 for both an ideal and an optical force model. Independent of the selected force model, it happens that $\beta \simeq e_\oplus$ for a wide range of variation of true anomaly. Within this range, the variation of α is nearly linear with ν_0, see Fig. 7.

2.6. Time variation of osculating orbit parameters

When the spacecraft covers a logarithmic spiral trajectory, the angular coordinate θ and the distance r may be expressed as explicit functions of the flight time t [18]. It will be shown now that a similar conclusion applies to the semimajor axis and argument of pericenter of the osculating orbit (recall, instead, that eccentricity and true anomaly are constant). Indeed, substituting Eq. (15) into (19) and integrating by separation of variables, the angular coordinate is found to be

$$\theta(t) = \nu_0 + \frac{2}{3}\,\cot\gamma\,\ln\left(1 + \frac{3}{2}\,k\,\sin\gamma\,\sqrt{\frac{\mu_\odot}{r_0^3}}\,t\right), \tag{49}$$

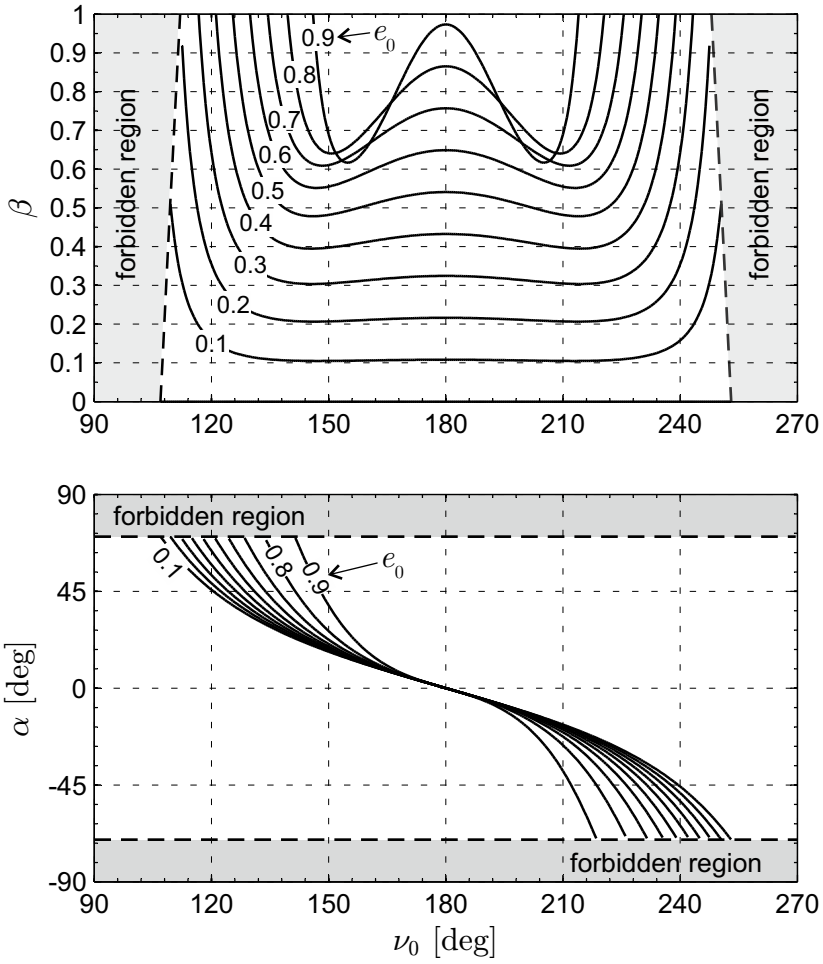

Figure 6: **Required pitch angle α and sail lightness number β as functions of ν_0 and e_0 for an optical force model.**

where r_0, γ, and k are given as a function of $\{e_0, \nu_0\}$ by Eq. (16), Eq. (17), and Eq. (34), respectively. Substituting then the last equation into Eq. (15), the Sun-spacecraft distance varies with time as

$$r(t) = r_0 \left(1 + \frac{3}{2}\, k\, \sin\gamma \sqrt{\frac{\mu_\odot}{r_0^3}}\, t\right)^{2/3}. \tag{50}$$

Finally, the semimajor axis and argument of longitude of the osculating orbit are immediately obtained from Eqs. (24) and (26) as

$$a(t) = a_0 \left(1 + \frac{3}{2}\, k\, \sin\gamma \sqrt{\frac{\mu_\odot}{r_0^3}}\, t\right)^{2/3} \tag{51}$$

and

$$\omega(t) = \frac{2}{3}\, \cot\gamma\, \ln\left(1 + \frac{3}{2}\, k\, \sin\gamma \sqrt{\frac{\mu_\odot}{r_0^3}}\, t\right). \tag{52}$$

Likewise, the ratio of the flight time t to the parking orbit period T_0, where $T_0 \triangleq 2\pi \sqrt{a_0^3/\mu_\odot}$, is given by

$$\frac{t}{T_0} = \frac{\left(1 - e_0^2\right)^{3/2}}{3\pi\, k\, \sin\gamma\, \left(1 + e_0\, \cos\nu_0\right)^{3/2}} \left\{\exp\left[\frac{3}{2}\, \tan\gamma\, (\theta - \nu_0)\right] - 1\right\}. \tag{53}$$

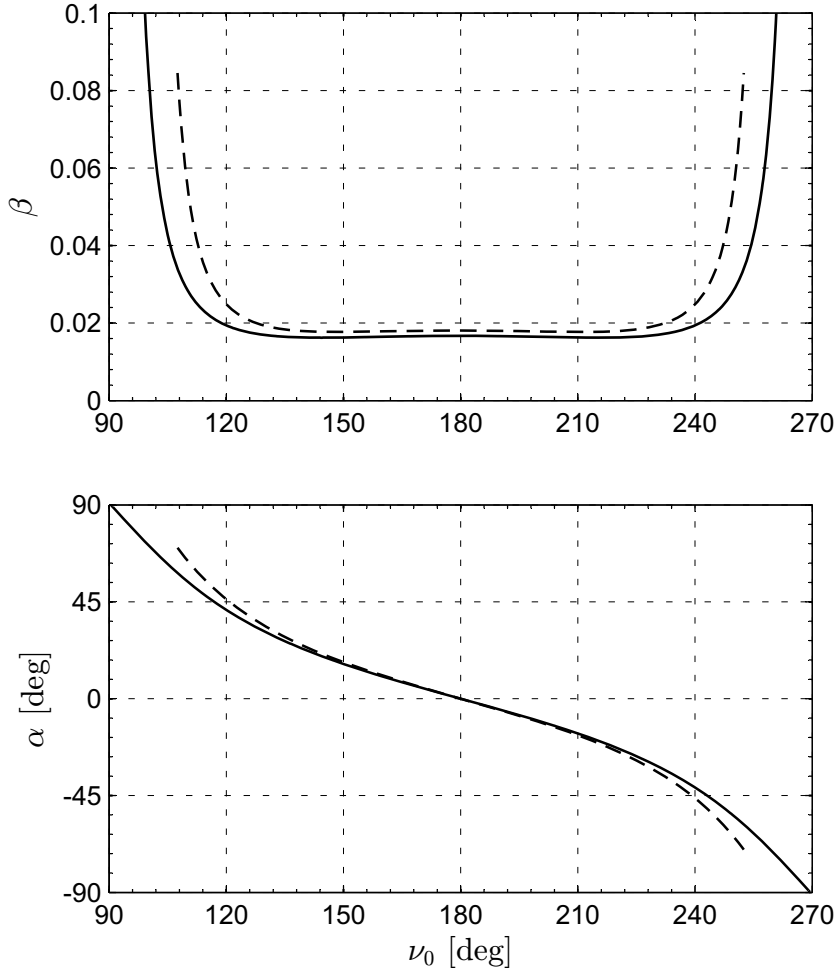

Figure 7: **Required pitch angle α and sail lightness number β as a function of ν_0 when $e_0 = e_\oplus = 0.0167$ for an ideal (solid line) and optical (dash line) force model.**

Note that, when $\nu = 180\,\text{deg}$ (and, therefore, $\gamma = 0$), from Eq. (34) the ratio t/T_0 becomes

$$\frac{t}{T_0} = \frac{(\theta - \nu_0)}{2\pi} \sqrt{\frac{(1+e_0)^3}{1-e_0}}. \tag{54}$$

This is an interesting scenario, in which the sail deployment coincides with the aphelion of the parking orbit, and the Sun-spacecraft distance is a constant of motion $r(t) = r_0 = a_0\,(1+e_0)$, see Eq. (15). In this special case, the logarithmic spiral degenerates into a non-Keplerian circular orbit [14], which is covered with an angular velocity less than that corresponding to a Keplerian circular orbit with the same radius r_0. Such an orbit is obtained using a Sun-facing sail ($\alpha = 0$, see Eq. (35)) with a lightness number $\beta = e_0/(b_1 + b_2 + b_3)$, see Eq. (36).

It is worth noting that the results obtained in this section are compatible with the hodograph representation described by [2], see the Appendix.

3. Mission application: orbit phasing

A possible application of the logarithmic spiral trajectory is an orbit phasing maneuver, which is performed when a spacecraft changes its angular coordinate, along a fixed heliocentric orbit, with respect to the

position it would have in case of Keplerian motion, after a given time interval. This kind of maneuver offers the possibility of suitably deploying a constellation of spacecraft along a working orbit, with the aim, for example, of studying the properties of the Sun and the solar wind by different vantage points, and providing an early warning against solar flares and mass ejections.

The adopted strategy consists in dividing the transfer trajectory into three phases, see Fig. 8. In the first one, the solar sail spacecraft is inserted into a logarithmic spiral branch, where the osculating orbit semimajor axis a varies according to Eq. (27), while the eccentricity e and the true anomaly ν remain unchanged, see Eqs. (25). Then, when the second phase starts, the sail is oriented edgewise to the Sun ($\alpha = \pm 90\,\mathrm{deg}$) so that the propulsive acceleration vanishes, and the spacecraft is inserted into a Keplerian arc. In this phase, the only varying orbital parameter is the true anomaly ν. When the latter reaches an assigned value, the third (and last) phase starts, and the sail is (backward) rotated in order to insert the spacecraft into another logarithmic spiral branch, whose aim is to bring the osculating orbit semimajor axis a back to its initial value. Since the osculating orbit eccentricity and true anomaly are constant in the third phase, the final values of a and e coincide with their corresponding initial values, while the angular position is different. Note also that, during the two logarithmic spiral arcs, the apse line of the osculating orbit rotates with the same angular velocity as that of the spacecraft, according to Eq. (26). Because the orbital orientation is required to remain unchanged at the end of a phasing maneuver, a total apse line rotation equal to an integer multiple of 2π must be enforced.

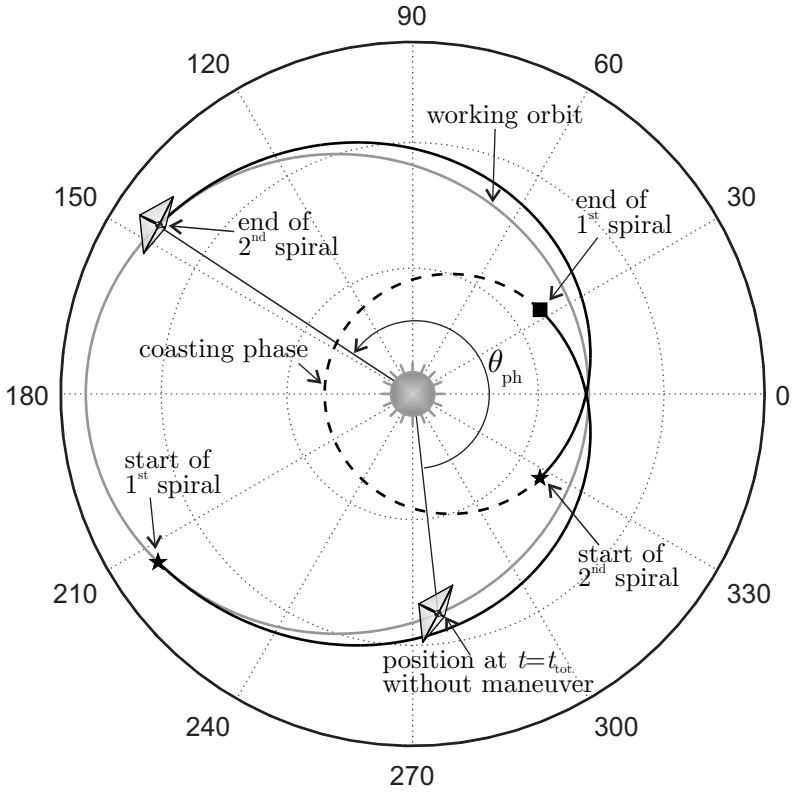

Figure 8: **Conceptual sketch of the orbit phasing mission scenario.**

To simplify the analysis, the rotation angle of the apse line is assumed to be the same in the first and third phase, each one contributing by a rotation angle equal to π. The total apse line rotation is therefore 2π, and the generalization to an integer multiple of 2π is straightforward. For exemplary purposes, consider a solar sail-based spacecraft initially placed along a heliocentric elliptic parking orbit with orbital parameters a_0, e_0, and ω_0. Also, let ν_0 be the spacecraft true anomaly at the beginning of the maneuver. Its flight path

angle γ_0 can be calculated by means of Eq. (17) as

$$\gamma_0 = \arctan\left(\frac{e_0 \sin\nu_0}{1 + e_0 \cos\nu_0}\right). \tag{55}$$

When the solar sail is deployed, the spacecraft is inserted into a logarithmic spiral trajectory where, as stated, it sweeps an angle equal to π, that is

$$\theta_1 = \nu_0 + \pi, \tag{56}$$

where subscript 1 indicates the end of the first phase. Accordingly, the apse line rotation at the end of the first spiral arc may be written as

$$\omega_1 = \pi. \tag{57}$$

Using Eqs. (25) and (27), the orbital elements at the end of the first phase are

$$a_1 = a_0 \, \exp\left(\pi \, \tan\gamma_0\right), \qquad e_1 = e_0, \qquad \nu_1 = \nu_0. \tag{58}$$

Note that, as expected, the osculating orbital eccentricity and true anomaly are constant, while the semimajor axis increases (decreases) when the flight path angle is positive (negative).

At the end of the first phase, which coincides with the beginning of the second phase, the solar sail propulsive acceleration is instantly set equal to zero with a suitable sail attitude maneuver, and the spacecraft is inserted into a Keplerian trajectory. Recalling the solution to Kepler's problem and using Eqs. (58), the orbital elements after the coasting phase are

$$a_2 = a_1 = a_0 \, \exp\left(\pi \, \tan\gamma_0\right), \qquad e_2 = e_1 = e_0, \qquad \omega_2 = \omega_1 = \pi, \tag{59}$$

where subscript 2 identifies the end of the second phase, when the spacecraft true anomaly is ν_2. The corresponding flight path angle is obtained from Eq. (17) as

$$\gamma_2 = \arctan\left(\frac{e_2 \sin\nu_2}{1 + e_2 \cos\nu_2}\right) = \arctan\left(\frac{e_0 \sin\nu_2}{1 + e_0 \cos\nu_2}\right). \tag{60}$$

The third phase starts when the solar sail is backward rotated, in order to insert the spacecraft into the second and final logarithmic spiral path. During this phase, the total swept angle is, again, equal to π, that is

$$\theta_3 = \nu_2 + \pi, \tag{61}$$

where subscript 3 indicates the end of the third phase (and of the whole maneuver). Accordingly,

$$\omega_3 = \omega_2 + \pi = 2\pi, \tag{62}$$

stating that the total rotation of the apse line during the whole maneuver is equal to 2π, as required. The expressions of the final osculating orbital parameters can be written using Eqs. (25), (27), and (59) as

$$a_3 = a_2 \, \exp\left(\pi \, \tan\gamma_2\right) = a_0 \, \exp\left[\pi \left(\tan\gamma_0 + \tan\gamma_2\right)\right], \qquad e_3 = e_2 = e_0, \qquad \nu_3 = \nu_2. \tag{63}$$

Since the phasing maneuver does not change the orbit shape, the final semimajor axis coincides with the initial one, or $a_3 = a_0$. Hence, the first of Eqs. (63) yields

$$\gamma_2 = -\gamma_0 \tag{64}$$

and, accordingly

$$\nu_2 = 2\pi - \nu_0. \tag{65}$$

Equation (64) shows the two spiral arcs to be symmetrical to each other, while Eq. (65) states that the final angular position of the coasting (Keplerian) phase is strictly related to the initial conditions.

It is now possible to investigate the feasibility of such a mission scenario. Firstly, the flight path angle γ_0

is more conveniently identified as γ (hence, $\gamma_2 = -\gamma$). The tangent of the flight path angle can be expressed as a function of the ratio of the final to the initial osculating semimajor axis of the first spiral branch a_1/a_0, by rewriting the first of Eqs. (58) as

$$\tan\gamma = \frac{\ln\left(a_1/a_0\right)}{\pi}. \tag{66}$$

Substituting Eq. (17) into Eq. (66) and denoting the (constant) eccentricity with $e \equiv e_0$, the result is

$$\frac{e\sin\nu_0}{1+e\cos\nu_0} = \frac{\ln\left(a_1/a_0\right)}{\pi}. \tag{67}$$

Solving Eq. (67) for the initial true anomaly ν_0 yields

$$\begin{cases} \nu_{0_A} = 2\pi - \arccos\left[\dfrac{-\tan^2\gamma/e - \sqrt{\tan^2\gamma\left(1-1/e^2\right)+1}}{1+\tan^2\gamma}\right] \\ \nu_{0_B} = 2\pi - \arccos\left[\dfrac{-\tan^2\gamma/e + \sqrt{\tan^2\gamma\left(1-1/e^2\right)+1}}{1+\tan^2\gamma}\right] \end{cases} \qquad \text{if} \quad a_1/a_0 < 1, \tag{68}$$

$$\nu_0 = \pi \qquad \text{if} \quad a_1/a_0 = 1, \tag{69}$$

$$\begin{cases} \nu_{0_A} = \arccos\left[\dfrac{-\tan^2\gamma/e - \sqrt{\tan^2\gamma\left(1-1/e^2\right)+1}}{1+\tan^2\gamma}\right] \\ \nu_{0_B} = \arccos\left[\dfrac{-\tan^2\gamma/e + \sqrt{\tan^2\gamma\left(1-1/e^2\right)+1}}{1+\tan^2\gamma}\right] \end{cases} \qquad \text{if} \quad a_1/a_0 > 1. \tag{70}$$

The special case $a_0 = a_1$ represents an apse line rotation at constant angular velocity, obtained by deploying the sail at the parking orbit aphelion and maintaining $\alpha = 0$ along the whole maneuver. Note that, in this case, a purely radial propulsive acceleration is required with $\beta R = e_0$, see Eqs. (35)–(36). However, it is clear that, in general, there are two possible values of ν_0 (subscripts A and B) for a given value of the ratio a_1/a_0, that is, for a given value of $\tan\gamma$, see Eq. (66). Note that, according to Eqs. (68) and (70), the initial conditions must meet the following constraints

$$\tan^2\gamma\left(1-1/e^2\right)+1 \geq 0, \tag{71}$$

$$\left|\frac{-\tan^2\gamma/e \pm \sqrt{\tan^2\gamma\left(1-1/e^2\right)+1}}{1+\tan^2\gamma}\right| \leq 1. \tag{72}$$

Equation (71) implies that

$$|\tan\gamma| \leq \frac{e}{\sqrt{1-e^2}}. \tag{73}$$

The inequality (73) is always satisfied, since $\arctan\left(e/\sqrt{1-e^2}\right)$ is the maximum value (in magnitude) reachable by the flight path angle. Note that ν_0 must also meet the constraint given by Eq. (38), otherwise a logarithmic spiral cannot be covered. Finally, for symmetry reasons, the insertion conditions on the second spiral are equivalent to those derived for the first spiral. To prevent the sail film from excessive thermal loads, a constraint on the perihelion distance r_{p1} is introduced, viz.

$$r_{p1} = a_1\left(1-e_1\right) \geq r_{\min}, \tag{74}$$

where $r_{\min}$ is the minimum admissible heliocentric distance. Using Eqs. (58), the latter inequality can be rewritten as

$$r_{p1} = r_{p0}\,\exp\left(\pi\,\tan\gamma\right) \geq r_{\min}, \tag{75}$$

where r_{p0} is the perihelion distance on the initial orbit. Since $r_{\min} < r_{p0}$, the constraint may become active

only if $\gamma \leq 0$, so Eq. (75) can be rearranged as

$$|\gamma| \leq \arctan\left[\frac{1}{\pi}\,\ln\left(\frac{r_{p0}}{r_{\min}}\right)\right]. \tag{76}$$

According to [20], a conservative value $r_{\min} = 0.4\,\text{au}$ is chosen for simulation purposes. Note that since the maximum magnitude of γ is $\arctan\left(e_0/\sqrt{1-e_0^2}\right)$, an equivalent version of (75) is

$$\frac{e_0}{\sqrt{1-e_0^2}} \leq \frac{1}{\pi}\,\ln\left[\frac{a_0\,(1-e_0)}{r_{\min}}\right]. \tag{77}$$

When the phasing maneuver ends, the spacecraft true anomaly is, of course, different from that obtained in a purely Keplerian motion. The difference between the two anomalies is the phase angle θ_{ph}, which can be calculated as follows. First, the total maneuver time t_{tot} is obtained as the sum of the flight times on each of the two logarithmic spirals t_{sp} and the coasting time on the Keplerian arc t_{c}. Indeed, the two spiral branches are symmetric, and the flight time is the same on both branches. From Eqs. (53) and (54), the ratio of the flight time t_{sp} on each spiral path to the initial orbital period T_0 is given by

$$\frac{t_{\text{sp}}}{T_0} = \frac{2\,(1-e^2)^{3/2}}{3\pi\,e\,\sin\nu_0\,(1+e\,\cos\nu_0)}\,\left[\left(\frac{a_1}{a_0}\right)^{3/2} - 1\right] \qquad \text{if} \quad a_1/a_0 \neq 1, \tag{78}$$

$$\frac{t_{\text{sp}}}{T_0} = \sqrt{\frac{(1+e)^3}{1-e}} \qquad \text{if} \quad a_1/a_0 = 1. \tag{79}$$

The ratio of the coasting time on the Keplerian arc t_{c} to T_0 is the result of a Kepler's problem with initial true anomaly ν_0 and final true anomaly $2\pi - \nu_0$, see Eq. (65), and the solutions are

$$\frac{t_{\text{c}}}{T_0} = \frac{1}{\pi}\,\left(\frac{a_1}{a_0}\right)^{3/2}\,(e_0\,\sin E_0 - E_0 + \pi) \qquad \text{if} \quad a_1/a_0 < 1, \tag{80}$$

$$\frac{t_{\text{c}}}{T_0} = 0 \qquad \text{if} \quad a_1/a_0 = 1, \tag{81}$$

$$\frac{t_{\text{c}}}{T_0} = \frac{1}{\pi}\,\left(\frac{a_1}{a_0}\right)^{3/2}\,(e_0\,\sin E_0 - E_0) \qquad \text{if} \quad a_1/a_0 > 1, \tag{82}$$

where $E_0 \in [0,\,2\pi]$ is the initial eccentric anomaly, given by

$$E_0 = 2\,\arctan\left[\sqrt{\frac{1-e}{1+e}}\,\tan\left(\frac{\nu_0}{2}\right)\right]. \tag{83}$$

Therefore, the total maneuver time t_{tot} is obtained as

$$t_{\text{tot}} = 2\,t_{\text{sp}} + t_{\text{c}}, \tag{84}$$

where the factor 2 accounts for the two spiral arcs. The angular position held by a spacecraft on the parking orbit at time t_{tot} may be calculated by solving an inverse Kepler's problem, viz.

$$E_{\text{K}} - e\,\sin E_{\text{K}} = \mod\left[2\pi\,\frac{t_{\text{tot}}}{T_0} + (E_0 - e_0\sin E_0)\,,\,2\pi\right], \tag{85}$$

where the final eccentric anomaly on the Keplerian orbit $E_{\text{K}} \in [0, 2\pi]$ is, as usual

$$E_{\text{K}} = 2\,\arctan\left[\sqrt{\frac{1-e}{1+e}}\,\tan\left(\frac{\nu_{\text{K}}}{2}\right)\right]. \tag{86}$$

The phase angle $\theta_{\rm ph}$ is given by the difference between the final true anomaly on the second logarithmic spiral and the final Keplerian true anomaly

$$\theta_{\rm ph} = 2\pi - \nu_0 - \nu_{\rm K}, \tag{87}$$

where $\nu_{\rm K}$ is calculated using Eq. (86).

Figure 9 shows the required lightness number β as a function of the phase angle $\theta_{\rm ph}$ for different values of eccentricity e, whereas Fig. 10 illustrates the dependance of $\theta_{\rm ph}$ on the ratio a_1/a_0. The range of admissible

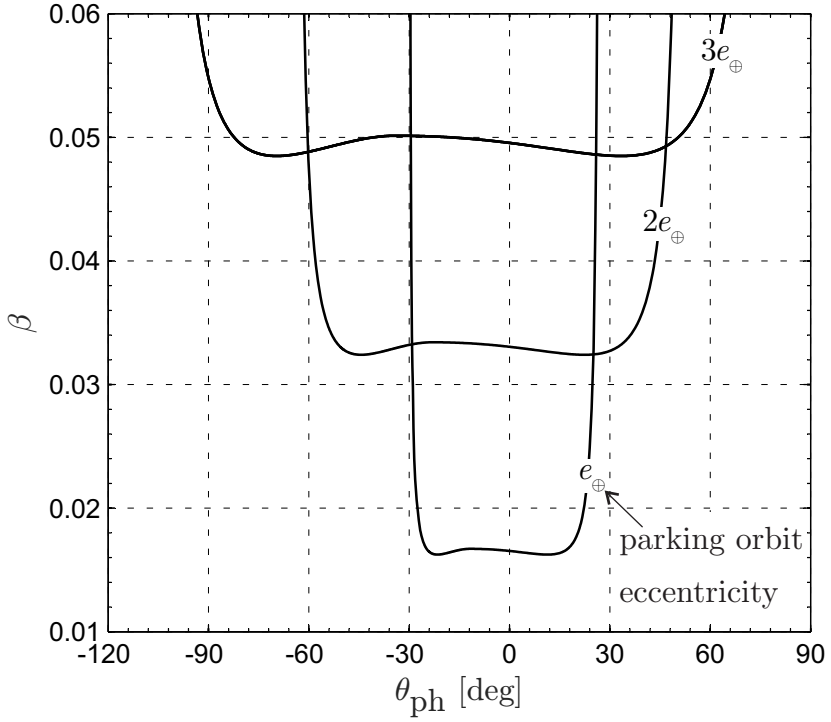

Figure 9: **Sail lightness number β as a function of the phase angle $\theta_{\rm ph}$ for $e = \{e_\oplus, 2\,e_\oplus, 3\,e_\oplus\}$.**

phase angles and the corresponding required lightness number tend to increase with the parking orbit eccentricity. Therefore, the feasibility of covering a logarithmic spiral trajectory for a solar sail spacecraft is limited by the sail performance, i.e., by the lightness number β. As far as the total flight time is concerned, Fig. 11 shows the variation of the ratio $t_{\rm tot}/T_0$ as a function of the phase angle $\theta_{\rm ph}$ and the parking orbit eccentricity. Figure 12 illustrates some orbit phasing maneuvers on the Earth's orbit (i.e. $a_0 = 1\,$au and $e = e_\oplus$) for two different values of a_1/a_0. Note that when the orbital eccentricity varies in the range illustrated in Figs. 9–12, the inequality (77) is always met.

4. Conclusions

A thorough analysis of the logarithmic spiral trajectory as a possible solution of the equations of motion for a solar sail-based spacecraft has been discussed. The relations between the parking orbit characteristics, the required insertion conditions, and the thermo-optical characteristics of the sail reflective film have been investigated, along with the angular and temporal variations of the osculating orbital elements. All these results have been obtained in terms of analytical closed-form expressions, and account for both an ideal and an optical sail force model. Such an outcome, in addition to the simple attitude control law required, makes the trajectory analysis for a solar sail on a logarithmic spiral simple and useful for a preliminary mission design. A potential mission scenario has been presented, in which a spacecraft placed on an elliptic heliocentric orbit can be phased by means of two logarithmic spiral-shaped branches and a Keplerian coasting

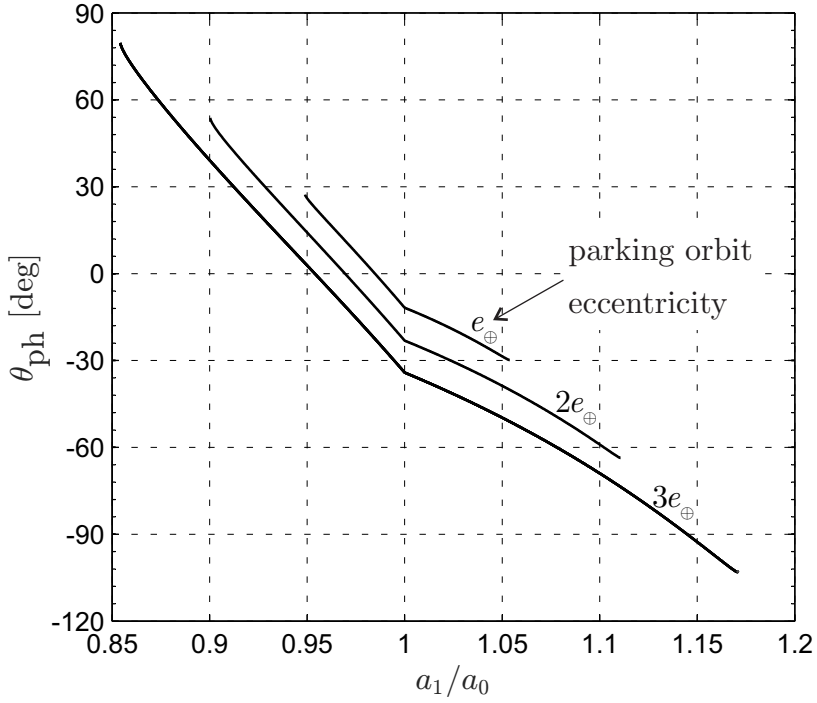

Figure 10: **Phase angle $\theta_{\rm ph}$ as a function of a_1/a_0 for $e = \{e_\oplus, 2\,e_\oplus, 3\,e_\oplus\}$.**

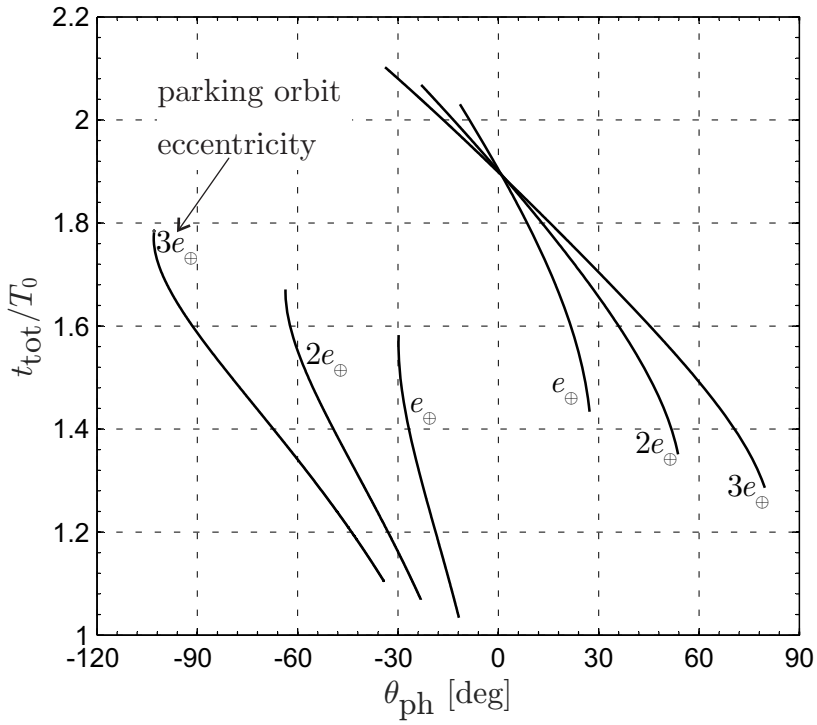

Figure 11: **Total maneuver time $t_{\rm tot}$ as a function of $\theta_{\rm ph}$ for $e = \{e_\oplus, 2\,e_\oplus, 3\,e_\oplus\}$.**

arc. Moreover, because a suitable curvature of the solar sail film could ensure a constant attitude in an

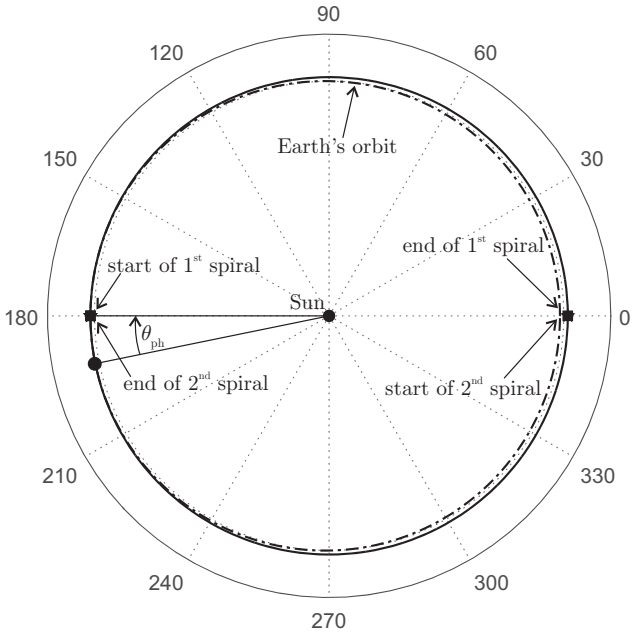

(a) $a_1/a_0 = 1$

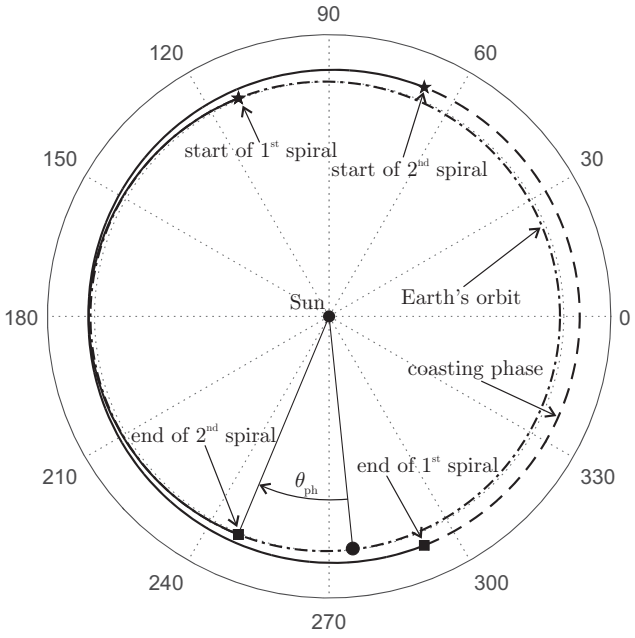

(b) $a_1/a_0 = 1.05$

Figure 12: **Orbit phasing maneuvers for $e = e_\oplus$ for different values of the ratio a_1/a_0.**

orbital reference frame, a natural extension of this work should include the effect of the sail billowing on the thrust vector characteristics. Another interesting future development is the analysis of a hybrid propulsion system, consisting of a solar sail and a conventional chemical thruster, which could exploit a combination of logarithmic-spiral arcs and impulsive maneuvers. This strategy would significantly increase the number of possible mission scenarios and overcome the limitations of the logarithmic spiral, at the expense of an increase of the total spacecraft mass.

Appendix - Hodograph representation of a logarithmic spiral trajectory

The characteristics of a logarithmic spiral trajectory can be analyzed by using the hodograph representation. In this context, the hodograph coordinates (x, y) are defined as [2, 21]

$$x \triangleq \frac{h\, v_\theta}{\mu_\odot}, \qquad\qquad y \triangleq \frac{h\, v_r}{\mu_\odot}, \tag{88}$$

where h is the magnitude of the spacecraft specific angular momentum. The equations of motion (3)-(4) may be rewritten as

$$\frac{\mathrm{d}x}{\mathrm{d}\theta} = 2\,\beta\,(b_2\,\cos^2\alpha\,\sin\alpha + b_3\,\cos\alpha\,\sin\alpha) - y, \tag{89}$$

$$\frac{\mathrm{d}y}{\mathrm{d}\theta} = \beta\,(b_2\,\cos^2\alpha\,\sin\alpha + b_3\,\cos\alpha\,\sin\alpha)\,\frac{y}{x} + x + \beta\,(b_1\,\cos\alpha + b_2\,\cos^3\,\alpha + b_3\,\cos^2\alpha). \tag{90}$$

The equilibrium points in Eqs. (89)-(90) are found by enforcing the necessary conditions

$$\frac{\mathrm{d}x}{\mathrm{d}\theta} = 0, \qquad\qquad \frac{\mathrm{d}y}{\mathrm{d}\theta} = 0. \tag{91}$$

Since α and β are both constant in a logarithmic spiral trajectory covered by a solar sail-based spacecraft, it is immediately found that x and y are constants of motion, together with the flight path angle γ, since

$$\gamma = \arctan\left(\frac{y}{x}\right). \tag{92}$$

On the hodograph plane, this result implies that the osculating orbital true anomaly and eccentricity are constant, see Fig. 13.

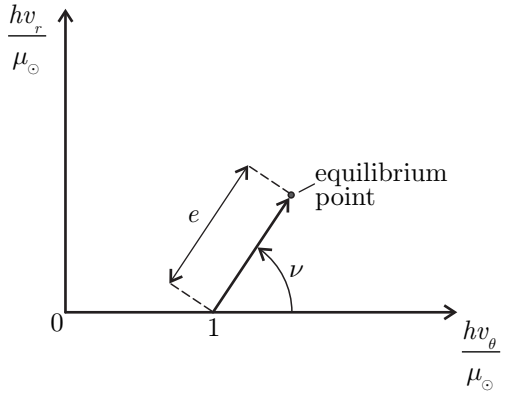

Figure 13: **Hodograph representation of a logarithmic spiral trajectory.**

Likewise, starting from the functions $\theta = \theta(t)$ and $r = r(t)$, it may be again verified that $x\,(t)$ and $y\,(t)$ are constant when a solar sail spacecraft covers a logarithmic spiral trajectory. In fact, bearing in mind Eqs. (49)-(50), Eqs. (88) give

$$x = (k\,\cos\gamma)^2\,, \qquad\qquad y = k^2\,\sin\gamma\,\cos\gamma, \tag{93}$$

where k and γ are constant.

References

[1] Bacon, R. H., 1959. Logarithmic spiral: An ideal trajectory for the interplanetary vehicle with engines of low sustained thrust. American Journal of Physics 27 (3), 164–165, doi: 10.1119/1.1934788.

[2] Battin, R. H., 1999. An Introduction to the Mathematics and Methods of Astrodynamics, Revised Edition. AIAA, 1801 Alexander Bell Drive, Reston, VA 20191, Ch. 3, pp. 126–127, ISBN: 1-56347-342-9.
[3] Betts, B., Nye, B., Vaughn, J., et al., January 17–20 2017. Lightsail 1 mission results and public outreach strategies. In: The 4th International Symposium on Solar Sailing. Kyoto Research Park, Kyoto, Japan.
[4] Betts, B., Spencer, D. A., Nye, B., et al., January 17–20 2017. Lightsail 2: Controlled solar sailing using a CubeSat. In: The 4th International Symposium on Solar Sailing. Kyoto Research Park, Kyoyo, Japan.
[5] Dachwald, B., Macdonald, M., McInnes, C. R., et al., July-August 2007. Impact of optical degradation on solar sail mission performance. Journal of Spacecraft and Rockets 44 (4), 740–749, doi: 10.2514/1.21432.
[6] Dachwald, B., Mengali, G., Quarta, A. A., et al., September-October 2006. Parametric model and optimal control of solar sails with optical degradation. Journal of Guidance, Control, and Dynamics 29 (5), 1170–1178, doi: 10.2514/1.20313.
[7] Funase, R., Kawaguchi, J., Mori, O., Sawada, H., Tsuda, Y., 23–26 April 2012. IKAROS, a solar sail demonstrator and its application to trojan asteroid exploration. In: 53rd Structural Dynamics and Materials Conference. Honolulu (HI), United States.
[8] Funase, R., Shirasawa, Y., Mimasu, Y., Mori, O., Tsuda, Y., Saiki, T., Kawaguchi, J., June 5–12 2011. Fuel-free and oscillation-free attitude control of IKAROS solar sail spacecraft using reflectivity control device. In: 28th International Symposium on Space Technology and Science. Okinawa, Japan.
[9] Heaton, A. F., Artusio-Glimpse, A. B., 31 August–2 September 2015. An update to the NASA reference solar sail thrust model. In: AIAA SPACE 2015 Conference and Exposition. Pasadena, California.
[10] Johnson, L., Castillo-Rogez, J., Dervan, J., McNutt, L., January 17–20 2017. Near earth asteroid (NEA) scout. In: The 4th International Symposium on Solar Sailing. Kyoto Research Park, Kyoto, Japan.
[11] Johnson, L., Whorton, M., Heaton, A., Pinson, R., Laue, G., Adams, C., March–April 2011. NanoSail-D: A solar sail demonstration mission. Acta Astronautica 68 (5–6), 571–575, doi: 10.1016/j.actaastro.2010.02.008.
[12] McInnes, C. R., November-December 1998. Passive control of displaced solar sail orbits. Journal of Guidance, Control, and Dynamics 21 (6), 975–982, doi: 10.2514/2.4334.
[13] McInnes, C. R., 2004. Solar Sailing Technology, Dynamics and Mission Applications. Springer-Praxis Series in Space Science and Technology. Springer-Verlag, Ch. 4, pp. 129–136.
[14] McKay, R. J., Macdonald, M., Biggs, J., McInnes, C., May-June 2011. Survey of highly-non-keplerian orbits with low-thrust propulsion. Journal of Guidance, Control, and Dynamics 34 (3), 645–666, doi: 10.2514/1.52133.
[15] McNutt, L., Johnson, L., Kahn, P., Castillo-Rogez, J., Frick, A., 4–7 August 2014. Near-earth asteroid (NEA) scout. In: AIAA SPACE 2014 Conference and Exposition. San Diego (CA), paper AIAA 2014-4435.
[16] Mori, O., Tsuda, Y., Shirasawa, Y., Saiki, T., Mimasu, Y., Kawaguchi, J., September 27–October 1 2010. Attitude control of IKAROS solar sail spacecraft and its flight results. In: 61st International Astronautical Congress. Prague, Czech Republic, paper IAC-10.C1.4.3.
[17] Niccolai, L., Quarta, A. A., Mengali, G., March 2017. Analytical solution of the optimal steering law for non-ideal solar sail. Aerospace Science and Technology 62, 11–18, doi: 10.1016/j.ast.2016.11.031.
[18] Petropoulos, A. E., Sims, J. A., June, 18–20 2002. A review of some exact solutions to the planar equations of motion of a thrusting spacecraft. In: 2nd International Symposium on Low-Thrust Trajectory (LoTus-2). Toulouse, France.
[19] Roa, J., Pelaez, J., Senent, J., 2016. New analytic solution with continuous thrust: generalized logarithmic spirals. Journal of Guidance, Control and Dynamics 39 (10), 2336–2351, doi: 10.2514/1.G000341.
[20] Sauer, Jr, C. G., 2000. Solar sail trajectories for solar polar and interstellar probe missions. Advances in the Astronautical Sciences 103 (1), 547–562 .
[21] Stewart, B., Palmer, P., Roberts, M., 2017. An analytical description of three-dimensional heliocentric solar sail orbits. Celestial Mechanics and Dynamical Astronomy 128, 61–74, doi: 10.1007/s10569-016-9740-x.
[22] Svitek, T., Friedman, L., Nye, W., Biddy, C., Nehrenz, M., 27 September – 1 October 2010 2010. Voyage continues – Lightsail-1 mission by the Planetary Society. In: 61st International Astronautical Congress. IAC, Prague, Czech Republic.
[23] Tsu, T. C., 1959. Interplanetary travel by solar sail. ARS Journal 29, 422–427 .
[24] Tsuda, Y., Mori, O., Funase, R., Sawada, H., Yamamoto, T., Takanao, S., Endo, T., Yonekura, K., Hoshino, H., Kawaguchi, J., July 2011. Achievement of IKAROS – Japanese deep space solar sail demonstration mission. In: 7th IAA Symposium on Realistic Advanced Scientific Space. Vol. 82. Aosta (Italy), pp. 183–188.
[25] Tychina, P. A., Egorov, V. A., Sazonov, V. V., July 1996. Quasi-optimal transfer of a spacecraft with a solar sail between circular heliocentric orbits. Cosmic Research 34 (4), 387–394 .
[26] Van Der Ha, J. C., Modi, V. J., February 1979. Long-term evaluation of three-dimensional heliocentric solar sail trajectories with arbitrary fixed sail setting. Celestial Mechanics 19 (2), 113–118, doi: 10.1007/BF01796085.
[27] Wokes, S., Palmer, P., Roberts, M., September–October 2008. Classification of two-dimensional fixed-sun-angle solar sail trajectories. Journal of Guidance, Control and Dynamics 31 (5), 1249–1258, doi: 10.2514/1.34466.
[28] Wright, J. L., 1992. Space Sailing. Gordon and Breach Science Publisher, Berlin, pp. 223–226.